JACS
JOURNAL OF THE AMERICAN CHEMICAL SOCIETY

Article

pubs.acs.org/JACS

# Quantification of the Surface Diffusion of Tripodal Binding Motifs on Graphene Using Scanning Electrochemical Microscopy

Joaquín Rodríguez-López, Nicole L. Ritzert, Jason A. Mann, Cen Tan, William R. Dichtel,* and Héctor D. Abruña*

Department of Chemistry and Chemical Biology, Cornell University, Ithaca, New York 14853-1301, United States

Supporting Information

**ABSTRACT:** The surface diffusion of a cobalt bis-terpyridine, $Co(tpy)_2$-containing tripodal compound (**1·2PF$_6$**), designed to noncovalently adsorb to graphene through three pyrene moieties, has been studied by scanning electrochemical microscopy (SECM) on single-layer graphene (SLG). An initial boundary approach was designed in which picoliter droplets (radii ~15−50 μm) of the tripodal compound were deposited on an SLG electrode, yielding microspots in which a monolayer of the tripodal molecules is initially confined. The time evolution of the electrochemical activity of these spots was detected at the aqueous phosphate buffer/SLG interface by SECM, in both generation/collection (G/C) and feedback modes. The tripodal compound microspots exhibit differential reactivity with respect to the underlying graphene substrate in two different electrochemical processes. For example, during the oxygen reduction reaction, adsorbed **1·2PF$_6$** tripodal molecules generate more $H_2O_2$ than the bare graphene surface. This product was detected with spatial and temporal resolution using the SECM tip. The tripodal compound also mediates the oxidation of a Fe(II) species, generated at the SECM tip, under conditions in which SLG shows slow interfacial charge transfer. In each case, SECM images, obtained at increasing times, show a gradual decrease in the electrochemical response due to radial diffusion of the adsorbed molecules outward from the microspots onto the unfunctionalized areas of the SLG surface. This response was fit to a simple surface diffusion model, which yielded excellent agreement between the two experiments for the effective diffusion coefficients: $D_{eff}$ = 1.6 (±0.9) × $10^{-9}$ $cm^2/s$ and $D_{eff}$ = 1.5 (±0.6) × $10^{-9}$ $cm^2/s$ for G/C and feedback modes, respectively. Control experiments ruled out alternative explanations for the observed behavior, such as deactivation of the Co(II/III) species or of the SLG, and verified that the molecules do not diffuse when confined to obstructed areas. The noncovalent nature of the surface functionalization, together with the surface reactivity and mobility of these molecules, provides a means to couple the superior electronic properties of graphene to compounds with enhanced electrochemical performance, a key step toward developing dynamic electrode surfaces for sensing, electrocatalysis, and electronic applications.

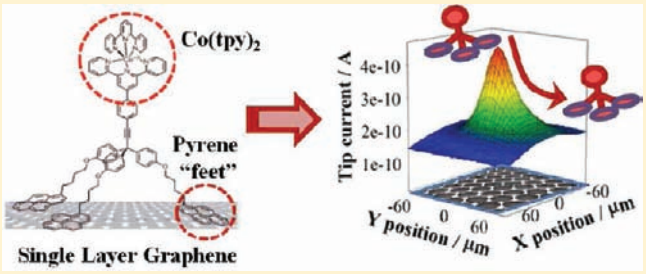


## INTRODUCTION

Here, we demonstrate that single layer graphene (SLG) allows the mobility of redox-enhancing molecular binders at its surface in an electrolytic medium. The superb physical, optical, and electronic properties[1−4] of single- and multilayer graphene motivate its fundamental study and development for applications including transparent electrodes,[5−8] resonators,[9,10] transistors,[11−16] and others. However, within an electrochemical context, SLG exhibits slow interfacial charge transfer kinetics at the graphene/solvent interface with many redox mediators, as do highly oriented pyrolytic graphite (HOPG) and carbon nanotubes.[17−21] This reactivity increases with the intentional generation of oxygenated defects,[22] nitrogen incorporation,[23] and in graphene oxide samples with abundant reactive edges and oxide sites,[24−29] but these modifications disrupt graphene's conjugation.[25] In contrast, noncovalent functionalization couples the superior electronic properties of SLG to adsorbed molecules with enhanced electrochemical activity. We recently introduced[30] the tripodal compound **1·2PF$_6$**, which consists of a Co(II) bis-terpyridine [$Co(tpy)_2$] redox center attached to a tetrahedral core bearing three pyrene "feet". The pyrene moieties interact strongly with the graphene surface[31] (Figure 1A), and this multivalent design results in kinetically stable monolayers that resist desorption under infinite dilution conditions.[30]

Although **1·2PF$_6$** molecules do not desorb readily from SLG, we hypothesized that they might diffuse over the two-dimensional carbon surface. Here we explore the surface mass transport properties of **1·2PF$_6$** on SLG by detecting its differential electrochemical activity with spatial and temporal resolution. Thus we designed two strategies, each based on the scanning electrochemical microscope (SECM),[32−34] for the electrochemical detection of the **1·2PF$_6$** surface concentration in real time, allowing its surface diffusion coefficient to be measured. In this work, we demonstrate the ability of adsorbed

**Received:** November 13, 2011
**Published:** March 12, 2012

   dx.doi.org/10.1021/ja2106724 | J. Am. Chem. Soc. 2012, 134, 6224−6236

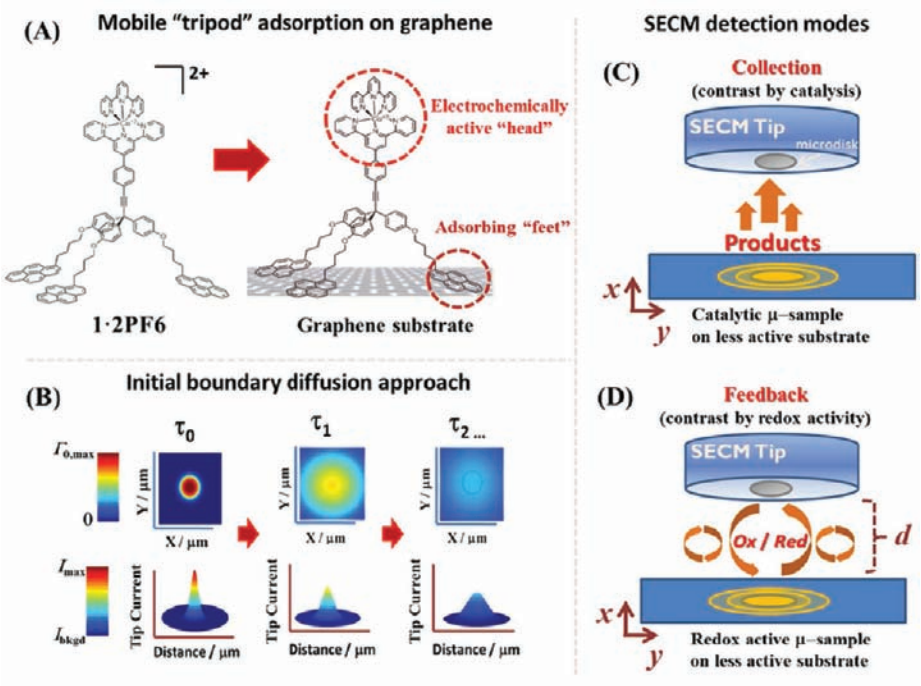


**Figure 1.** Strategy for characterizing the surface diffusion of a tripodal compound on graphene using SECM. (A) Chemical structure of tripodal compound **1·2PF$_6$** and its proposed mode of adsorption onto SLG. (B) Initial boundary approach for measuring the surface diffusion of **1·2PF$_6$**, initially confined to a few micrometers-sized spot, by detecting a decrease in its electrochemical activity as a result of radial diffusion onto the bulk surface. Schematics of the complementary substrate generation/tip collection (C) and feedback modes (D) of SECM. In each case, the SECM microelectrode (radius $a$) is positioned at a distance $d$ from the substrate and scanned in the $x$ and $y$ directions to produce a spatially and temporally resolved reactivity image.

functionalities to modify the electrochemical activity of graphene and exploit the dynamic nature of noncovalent $\pi$-stacking interactions. Controlling the surface diffusion of molecular electrocatalysts[35] on a model carbon support, such as graphene, is an intriguing possibility for designing efficient catalytic platforms and studying association phenomena,[35,36] for which dynamic interactions between electrocatalysts may benefit the product selectivity or catalytic performance. These and other cooperative properties might emerge from the ability of the surface to present dynamic combinations of functional groups. Finally, functionalizing graphene with $[Co(tpy)_2]$ or other redox couples using motifs that bind with predictable and well-defined orientations might also facilitate future studies of molecular electronic phenomena.[37,38]

Relatively few techniques can measure surface diffusion coefficients at the solid/liquid or solid/electrolyte interface. Electrochemical scanning tunneling microscopy (EC-STM) may be used in principle,[39,40] but this technique is uncommon because of the difficulty of imaging in liquids at room temperature.[41] In most instances, only qualitative data are obtained or inferred.[42] STM has been used at cryogenic temperatures to study molecular adsorption on graphene under more favorable conditions.[43,44] Nuclear magnetic resonance has been applied to a limited subset of samples, such as lipid bilayers[45,46] or to suspended samples of nanoparticle electrocatalysts.[47,48] Fluorescence measurements,[49,50] such as the widely used fluorescence recovery after photobleaching method (FRAP),[51−53] in which the time dependence of the fluorescence restoration of a small photobleached spot is monitored, might also be used. However graphene oxide, reduced graphene oxide, and pristine SLG strongly quench organic dyes[54−57] and semiconductor nanocrystals,[58] likely rendering these surfaces incompatible with the FRAP approach. The limitations of the above techniques motivated us to develop an electrochemical method for characterizing the surface diffusion of **1·2PF$_6$** on SLG. The use of SECM for measuring surface diffusion coefficients was pioneered by Unwin[59] and co-workers at the water/air interface, first by taking advantage of acid−base equilibria[60−62] to use the generation/collection modes to study proton diffusion along Langmuir monolayers and later through feedback measurements using redox-active amphiphiles.[63] Effective diffusion coefficients for charge transfer across thin redox-active layers were also measured using an electrochemical analogue of FRAP experiments.[64−66] These electrochemical experiments require an inert supporting interface because it is otherwise difficult to deconvolve the SECM response to the background activity and lateral conductivity of the electrode[67,68] from charge transport or molecular diffusion. The low interfacial activity of graphene for several redox mediators provides the requisite low background over which the electrochemically active tripod molecules can be readily detected. Other complications that might obscure a linear SECM response to variations in the molecular surface concentration, such as a large self-exchange rate between adjacent redox centers,[69] were circumvented in this work through the judicious choice of the Co(II/III) redox couple, whose slow self-exchange rate[70,71] originates from an unfavorable spin conversion.[72,73] Likewise, we previously found that **1·2PF$_6$** exhibits Langmurian adsorption onto the SLG surface, which suggests that interactions between adjacent molecules are sufficiently weak to not complicate the surface diffusion analysis.[30]

Our experimental approach (Figure 1B) relies on characterizing the diffusion of the tripodal compound **1·2PF$_6$** radially


dx.doi.org/10.1021/ja2106724 | J. Am. Chem. Soc. 2012, 134, 6224−6236

outward from a monoloayer initially deposited as a small microspot. A droplet of the **1·2PF$_6$** solution of appropriate concentration to form a monolayer is dispensed as a microspot of radius $b$ onto the graphene surface, forming an initial boundary with (ideally) a uniform concentration of the tripod upon drying. When immersed in an electrolyte ($t = \tau_0$) that disfavors the desorption of the tripod but allows some degree of solvation of the [Co(tpy)$_2$] complex, the molecule diffuses outward onto the bare graphene surface. The SECM tip interrogates the electrochemical activity of the surface, or of products flowing outward from it, with spatial resolution and records "electrochemical snapshots" that describe the time evolution of the microspot. The microspot's activity decreases over time ($t = \tau_1, \tau_2, ..., \tau_x$) due to the radial dilution of the mobile **1·2PF$_6$** molecules on the surface. The decrease in the analytical signal at the center of the spot is fit to a surface diffusion model, yielding a macroscopic effective surface diffusion coefficient, $D_{eff}$.

Two complementary modes of SECM were used to differentiate the activity of **1·2PF$_6$** from the unfunctionalized SLG electrode. In the first (Figure 1C), a catalytic reaction triggered by the Co(tpy)$_2$ moiety generates homogeneous products that are collected at the tip.[74] Specifically, we used the oxygen reduction reaction (ORR) under kinetic control, eqs 1 and 2,[75] and showed that adsorbed **1·2PF$_6$** is able to generate more $H_2O_2$[35,76] than the bare SLG. The Pt tip detects this peroxide through the inverse electrochemical process. $H_2O_2$ imaging using SECM has been used previously to characterize immobilized enzymes[77−80] and to evaluate the activity of electrocatalysts.[81−83]

$$O_2 + 2e^- + 2H^+ \rightarrow H_2O_2 \quad (1)$$

$$O_2 + 4e^- + 4H^+ \rightarrow H_2O \quad (2)$$

In the second mode (Figure 1D), feedback measurements directly assess the electrochemical activity of the tripodal molecules at the graphene/solution interface. Such feedback measurements of molecular species have been obtained at diverse interfaces, including self-assembled monolayers,[84] enzyme reactive sites,[85] intercalated DNA,[86] dye-sensitized solar cells,[87] and biological cells.[88] Here, a redox mediator in solution is activated at the tip, e.g. Ox + e$^-$ → Red, where Ox and Red are the oxidized and reduced mediator species, respectively. The substrate is held at a constant oxidizing potential such that each of the adsorbed Co(tpy)$_2$ redox centers are in the Co(III) oxidation state. The activated mediator, Red, diffuses to the surface, where it is oxidized by the Co(III) tripodal molecules to form Ox and a bound Co(II) species that is rapidly reoxidized to Co(III) by the activated surface. Ox diffuses back to the tip, where it is reactivated, and the repetition of these processes establishes a feedback current, which is measured at the tip. This feedback current is quantitatively related to an effective exchange rate constant that is directly proportional to the surface concentration of the adsorbed species.[84] The time evolution of the surface concentration is modeled to obtain $D_{eff}$ as described for the above generation/collection scheme. Fe(II/III) complexes were chosen as mediators since they are relatively insensitive to electrochemical activation at the basal plane of HOPG[89,90] and have shown good chemical identification of adsorbed species in contrast to the competing electrode activation.[91]

## EXPERIMENTAL SECTION

**Chemicals.** The tripodal compound **1·2PF$_6$** (Figure 1A) was synthesized using our previously reported procedures.[30] Aqueous experiments were carried out with deionized water from a Millipore system. Chemicals used as received were potassium phosphate monobasic, potassium chloride (KCl), isopropanol (IPA), dimethylformamide (DMF), dichloromethane (DCM), glycerol (GLY), ethanol (EtOH), and acetone from Mallinckrodt; agar and ethylenediamine-tetraacetic acid ferric sodium salt (FeEDTA) from Sigma; potassium phosphate dibasic trihydride, tetrahydrofuran (THF), and anisole from Aldrich; potassium hexacyanoferrate (ferricyanide) and nitric acid from Fisher; tetrabutylammonium perchlorate (TBAP) from Fluka; hydroxymethylferrocene and Cu foil (0.025 mm thick, 99.8%) from Alfa; glacial acetic acid, acetone, and isopropanol for graphene synthesis from VWR. For the fabrication of SECM tip electrodes, soft glass capillaries (FHC, Inc.) and 25 $\mu$m diameter platinum (99.99%) microwire (Goodfellow) were used and polished on microcloth polishing pads (Buehler). Silver, gold, tungsten, and indium wires were supplied by Sure Pure metals. The electrochemically active copolymer poly(vinylpyridine)/poly(vinylferrocene)[92] (PVP/PVF) 2:1 was used from an available batch. Reference electrodes were homemade Ag/AgCl in saturated KCl, and all potentials are quoted versus this reference. The reference was used with disposable 3% agar jelly/0.2 M potassium nitrate salt bridges to prevent silver ion and chloride contamination in the electrochemical cell. Gold was used as counter electrode and was sonicated in acetone and rinsed with water before use. For experiments with highly oriented pyrolytic graphite, HOPG SPI-2 grade (Structure Probe Inc.) was freshly cleaved before experiments using adhesive tape and then rinsed in the electrochemical cell using IPA. Graphene was obtained through chemical vapor deposition on Cu substrates and later transferred onto Si/SiO$_2$ chips (see Supporting Information, Figure S1).

**Electrochemical Measurements.** All electrochemical and SECM measurements were performed with a CHI 900 SECM station. A homemade Teflon electrochemical cell with an active window of 0.2 cm$^2$, in which the graphene or HOPG substrate electrodes were sandwiched between an O-ring in the Teflon body and the PMMA base, was used for SECM and three-electrode measurements. For conventional three electrode experiments in organic solvents, either graphene or HOPG was used as the working electrode, with a Ag wire as a reference and a Au wire as counter electrode. Experiments in which **1·2PF$_6$** adsorption was monitored, with the electrode later transferred to an aqueous environment, consisted in using <5 $\mu$M tripod in THF or DMF with 0.1 M TBAP as supporting electrolyte and running cyclic voltammograms (CV) to verify the adsorption of the tripod and to calculate its coverage. In order to study the behavior of the tripod in an aqueous environment, the cell was thoroughly rinsed with blank solvent (THF or DMF) to remove excess tripod and organic supporting electrolyte, then rinsed with IPA at least once (to recreate the conditions of the blank electrodes), and then thoroughly rinsed with deionized water to remove excess solvents. Finally phosphate buffer (0.2 M, pH 7) was introduced as the aqueous electrolyte. While inevitable losses were observed during this procedure, **1·2PF$_6$** could be detected and quantified using CV in the aqueous solution. Adsorption of PVP/PVF for feedback and control experiments was carried out by exposing the substrate electrodes to a solution of 0.1 mg/mL of the polymer in EtOH and then rinsing with copious amounts of $H_2O$.

**Tripod Microspots on Graphene and HOPG.** Microarrays of drops of **1·2PF$_6$** solution were dispensed on graphene and HOPG using a picoliter dispenser with a 30-$\mu$m diameter orifice (Microfab Inc. Plano, Texas) controlled by a homemade circuit with output gain of 20X using two OPA445AP High Voltage FET-Input operational amplifiers (Burr-Brown products from Texas Instruments).[93] The dispenser was operated using a synthesized function generator model DS345 (Stanford Research Systems) and an oscilloscope model TDS 210 (Tektronics) and powered by two batteries at ±30 V. **1·2PF$_6$** was dissolved in a mixture of DMF/GLY 10:1 (intended to dissolve the tripod with a workable viscosity and low evaporation rate at room


dx.doi.org/10.1021/ja2106724 | J. Am. Chem. Soc. 2012, 134, 6224−6236

temperature) and was deposited by applying two consecutive pulses of 25 $\mu$s (20 kHz) at 44 V (input of 2.2 V). This deposition procedure typically yielded droplets of radius $b \approx 50$ $\mu$m as determined by optical microscopy. A calibration experiment (same solvent and parameters) that dispensed 100 times a solution of hydroxymethylferrocene (0.1 M) into a droplet (50 $\mu$L) of phosphate buffer was analyzed by steady state voltammetry using a 25-$\mu$m microelectrode in a two-electrode configuration. This calibration showed that each dispensing cycle produced droplets of 177 ± 8 pL, i.e., flattened hemispheres with radius $b \approx 50$ $\mu$m and height $h \approx 35$ $\mu$m. Using this information, the concentration of **1·2PF$_6$** was chosen to deliver the desired amount of adsorbate to the SLG surface. For example, [**1·2PF$_6$**] = 45 $\mu$M provides an approximate coverage of 104 pmol/cm$^2$ within each spot, which exceeds the ~70 pmol/cm$^2$ required for the first plateau observed in the isotherm for **1·2PF$_6$** on graphene but is lower than a more compact layer observed at ~140 pmol/cm$^2$. A slight excess is desirable to account for possible losses in the dispensing process[94] but much larger excesses, e.g., 5-fold monolayer equivalents, caused precipitation of **1·2PF$_6$** on the SLG surface and the inability to perform SECM measurements (i.e., a lower activity of spots is observed compared to the SLG substrate). Typical arrays of tripod spots were deposited on graphene or HOPG electrodes with interspot distances between 300 and 600 $\mu$m. The arrays were dried at 50 °C in an oven at ambient pressure for ~1 h before imaging. Successful images were typically obtained from arrays where no residue was evident on the graphene substrate upon microscopic inspection.

**SECM Experiments.** SECM experiments used a four electrode configuration. All SECM experiments were performed using a sharpened 25-$\mu$m diameter Pt microdisk SECM tip with an RG ≈ 7 (closest approach on glass $d_0 \approx 1.5$ $\mu$m) sealed in soft glass using reported procedures.[33] For imaging experiments, the time at which the solution was introduced into the cell and wetted the substrate electrode was defined as $t = 0$. The SECM tip was approached to the surface and positioned at a tip/surface distance of 10 $\mu$m. A first extended image or several lateral scans were performed at relatively high scan rate (e.g., 125 $\mu$m/s in steps of ~15–25 $\mu$m) to locate an active spot. Subsequent images were obtained at more moderate scan rates and higher resolution (e.g., 50 $\mu$m/s in steps of 6–10 $\mu$m). An accumulated uncertainty in the time assigned to each image (i.e., the maximum intensity of the image) is estimated to be ~100 s because of changes in the position of the spot due to a slight drift in the motors. All times shown in images are thus rounded to the nearest 100 s. All approach curves and tip positioning procedures were analyzed using reported expressions.[95]

For $H_2O_2$ collection experiments, the electrolyte was air-saturated aqueous phosphate buffer (0.2 M, pH = 7).[96] The tip was positioned in the negative feedback mode using $O_2$ as mediator (typical $i_{T,inf}$ = 7 nA). Unless otherwise noted, for $H_2O_2$ collection experiments, the substrate was biased to a potential $E_S = -0.6$ V vs Ag/AgCl and the tip to $E_T = 0.6$ V vs Ag/AgCl (i.e., ~1.22 V vs RHE, an optimum potential for $H_2O_2$ collection at Pt).[81] Occasional cleaning of the tip was performed between images by cycling between 0.8 and −0.6 V vs Ag/AgCl to prevent fouling, although no significant improvement was observed in relatively clean environments. Potassium ferricyanide (1–2 mM) dissolved in aqueous phosphate buffer (0.2 M, pH 7) was used for feedback imaging experiments. For graphene electrodes, the tip, $E_T$ = −0.1 V vs Ag/AgCl, was positioned by a negative feedback-like approach curve obtained with the substrate at open circuit (Supporting Information Figure S2).[97] For feedback experiments on HOPG, a positive feedback approach curve was also used to verify adequate positioning. During imaging, the substrate electrodes were biased to $E_S$ = 0.4 V vs Ag/AgCl unless otherwise noted. Conditions for the supporting experiments with FeEDTA as mediator are described in the Supporting Information.

**Simulations and Experimental Considerations.** Digital simulations of the surface diffusion problem coupled to the SECM conditions were performed using the COMSOL Multiphysics 3.5a software, which implements the finite element method to solve the required kinetic and diffusion coupled equations. A complete description of the simulation conditions for the G/C and feedback schemes is given in the Supporting Information.

Figure 2 shows the temporal evolution of the surface concentration of a species with a homogeneous surface concentration ($\Gamma_0$) that is

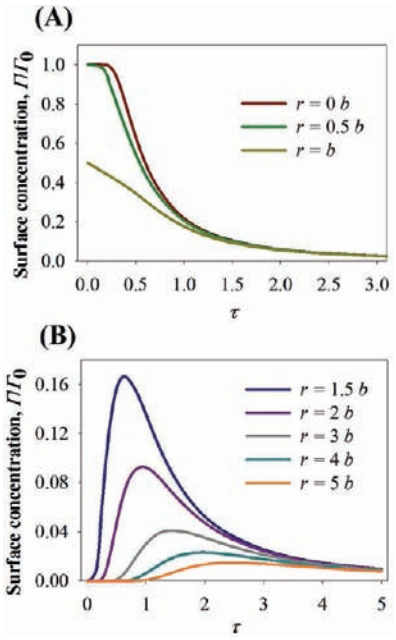


**Figure 2.** Master curves for the surface concentration changes associated with the two-dimensional diffusion of adsorbed molecules from a circular area with uniform initial concentration $\Gamma_0$ and radius $b$ outward onto a blank, bulk surface. The different curves indicate selected positions in the radial coordinate $r$, and the horizontal axis represents the normalized time $\tau$ (eq 3). The curves in panel A correspond to coordinates within the initial boundary, and the curves in panel B correspond to coordinates outside the initial boundary.

radially diffusing from an initially confined circular microspot (radius $b$). The microspot is surrounded by a semi-infinite blank surface with radius $20b$ and the diffusing species exhibits a uniform surface diffusion coefficient $D$ (i.e., independent of coverage and intermolecular interactions). The response is modeled using a radial coordinate $r$, where $r = 0$ represents the center of the microspot. The results of these simulations are displayed as a series of master curves that describe the temporal evolution of the surface concentration of the diffusing species relative to its initial value at the center of the microspot ($\Gamma/\Gamma_0$) at each of several normalized distances $r/b$ from the center. A dimensionless time $\tau$ is introduced as shown in eq 3:

$$\tau = \frac{\sqrt{Dt}}{b} \tag{3}$$

where $D$ is the diffusion coefficient of the species, $t$ is time, and $b$ is the radius of the microspot. The conditions tested include $1 \times 10^{-4}$ cm$^2$/s > $D$ > $1 \times 10^{-16}$ cm$^2$/s (1 cm$^2$/s = $1 \times 10^{-4}$ m$^2$/s), 1000 $\mu$m > $b$ > 0.001 $\mu$m (1 $\mu$m = $1 \times 10^{-6}$ m), and their respective times (s) such that $5 > \tau > 0$. Figure 2A,B shows the concentration profiles for the coordinates inside and outside the original area of the microspots, respectively. The concentration inside of the spot shows a continuous decrease as a consequence of radial diffusion, whereas the positions outside of the spot show a concentration front that increases and then vanishes upon further radial dilution.

Two observations relevant to our SECM measurements warrant further discussion. First, the steepest change in concentration and therefore electrochemical signal occurs at the center of the microspot, where the concentration drops to ~25% of its original value in one time period. This finding suggests that measuring the surface concentration as a function of time at the center of the microspot is


dx.doi.org/10.1021/ja2106724 | J. Am. Chem. Soc. 2012, 134, 6224–6236

likely to be the most effective strategy for characterizing the molecular diffusion process. Second, the changes within the original area of the spot follow closely those of the center while the changes outside the original area of the spot are not sufficient to supply more than ~10% of the original concentration to radii larger than $2b$ as a consequence of radial dilution of the species. Therefore, it is expected that only a modest broadening of the signal will be observed.

In utilizing the dimensionless time parameter ($\tau$), these simulations also highlight the interplay between the size of the spot deposited, the expectations on the value of $D$, and the absolute time and time resolution available for the experiment. For example, for $D = 1 \times 10^{-9}$ cm$^2$/s (a value between a typical solution diffusion coefficient, $D = 1 \times 10^{-5}$ cm$^2$/s, and that of a low surface diffusion coefficient, $D = 1 \times 10^{-13}$ cm$^2$/s, approaching diffusion in solids)[47] with a spot of radius $b = 50$ $\mu$m and for times $\tau < 1$, the absolute measuring time would conveniently be 25,000 s (e.g., enough for positioning the tip and obtaining several images), in contrast to 2.5 s if $b = 500$ nm, which would be experimentally difficult to probe through SECM imaging. Finally, in SECM experiments, the size of the tip affects the spatial and temporal resolution of the measurement. Scans performed with relatively large tips, e.g., $a > 5$ $\mu$m, allow for a fast screening of a given area (e.g., if $b = 50$ $\mu$m) at the expense of a convoluted signal from the area that is projected below the tip. Smaller tips could correlate directly the concentration profile at the substrate to the tip response but are more challenging to implement in a time-sensitive experiment. In this study we opted for the former option and solved the convoluted tip response by fitting to widely implemented computer simulations for SECM studies.

## RESULTS AND DISCUSSION

**$H_2O_2$ Collection Experiments.** We previously characterized the monolayer formation, desorption, and electrochemical behavior of the pyrene-based tripodal compound **1·2PF$_6$** on SLG.[30] Its Co(II/III) redox center exhibits quasi-reversible electrochemical kinetics at scan rates between 0.1 and 3.0 V/s with a standard potential $E^0 = -0.2$ V vs ferrocene. The slower rate of electron transfer between graphene and **1·2PF$_6$** (standard rate constant $k^0 = 13.5$ s$^{-1}$) relative to that of a model compound bearing a single pyrene moiety ($k^0 = 18$ s$^{-1}$) suggested that the tripodal motif projects its [Co(tpy)$_2$] complex away from the graphene surface. Finally, monolayers of **1·2PF$_6$** resist desorption when transferred to fresh THF/$NH_4PF_6$ electrolyte solution. Here, our SECM experiments are performed in aqueous electrolyte, in which **1·2PF$_6$** is insoluble and the strength of aromatic stacking interactions is maximized, making its desorption from SLG even less likely. As such, our measurements of the surface diffusion dynamics of **1·2PF$_6$** are minimally complicated by transport mechanisms other than lateral translation across the surface (e.g., desorption-convection). Preliminary experiments performed at the basal plane of freshly cleaved HOPG electrodes (analogous to the graphene surface) confirm that **1·2PF$_6$** is active in an aqueous environment (Figure 3) and remains strongly bound to the surface in aqueous electrolyte. At the same scan rate (0.1 V/s), a similar peak splitting $\Delta E_p \approx 100$ mV is observed in both THF and aqueous phosphate buffer, suggesting that the adsorption mode and orientation of the tripod is similar in both solvents.

A differential electrochemical response between adsorbed **1·2PF$_6$** and bare SLG is necessary to detect **1·2PF$_6$** using SECM. Qualitative collection of $H_2O_2$ at a Pt SECM tip originating from the ORR over HOPG and SLG electrodes in the presence and absence of **1·2PF$_6$** monolayers showed sufficient activity differences to provide this contrast (Figure 4). The onset for ORR on Pt in phosphate buffer occurs at ~0.15 V vs Ag/AgCl (~0.77 V vs RHE), and thus the reaction

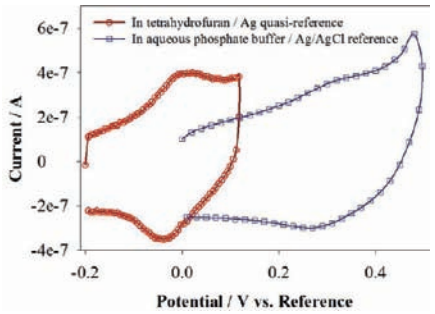


**Figure 3.** Cyclic voltammograms of **1·2PF$_6$** adsorbed on the basal plane of HOPG (initial surface concentration = 20 pmol/cm$^2$). The left voltammogram (red curve) was obtained in a 0.1 M TBAP in THF supporting electrolyte. The right voltammogram (blue curve) was obtained in phosphate buffer (0.2M, pH = 7) after rinsing the surface with THF, IPA, and $H_2O$.

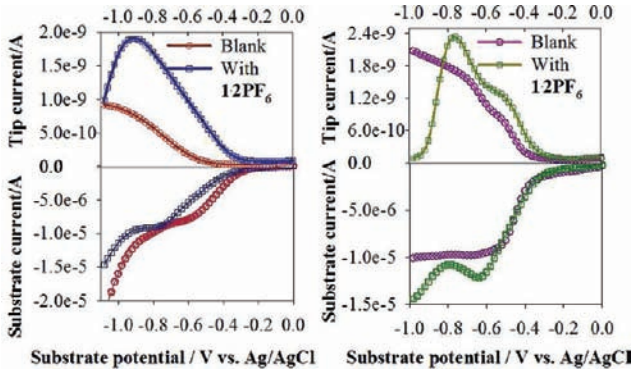


**Figure 4.** Substrate generation/tip collection curves for $H_2O_2$ generated during the oxygen reduction reaction performed in an air-saturated phosphate buffer (0.2 M, pH = 7) at a large-area (left) graphene electrode (**1·2PF$_6$** coverage =23 pmol/cm$^2$) or (right) HOPG electrode (**1·2PF$_6$** coverage = 28 pmol/cm$^2$). $H_2O_2$ collection at the SECM tip ($a = 12.5$ $\mu$m Pt, RG ≈ 7) was performed at $E_T = 0.6$ V vs Ag/AgCl at an interelectrode distance $d = 10$ $\mu$m. The linear sweep of the substrate voltage was performed at 10 mV/s.

presents a considerable overpotential on both bare SLG and HOPG. Inconsistencies in the rising portion of the curves for oxygen reduction (lower panels) were observed in different batches of graphene (Supporting Information Figure S3), possibly because of small amounts of residual metal ions from the fabrication process (e.g., Cu, Fe). Nevertheless, the output of $H_2O_2$ on both graphene and HOPG always increased following adsorption of **1·2PF$_6$**. This increase was not observed when the electrodes were exposed to organic electrolyte lacking **1·2PF$_6$**. Furthermore, Co complexes are known to form $H_2O_2$ during the ORR.[35,75,76] The $H_2O_2$ output curves (Figure 4) for graphene and HOPG show common features when **1·2PF$_6$** is present. Each curve shows a rise to a maximum $H_2O_2$ output, followed by a sharp decrease at increased overpotentials, which likely reflects a change in the predominant mechanism from the two-electron (eq 1) to the four-electron route (eq 2). In order to use $H_2O_2$ generation/collection to describe changes in the distribution of **1·2PF$_6$** on the electrode surface, the electrochemical reaction must operate under kinetic control, i.e., at low overpotentials, such that the rate of reaction is proportional to the molecular surface concentration. Compared to a bare glassy carbon surface (Supporting Information Figure S4), both **1·2PF$_6$**-modified SLG and HOPG produce less $H_2O_2$ at potentials positive of $E_S = -0.8$ V vs Ag/AgCl ($i_{T,max} = 3$ nA


dx.doi.org/10.1021/ja2106724 | J. Am. Chem. Soc. 2012, 134, 6224–6236

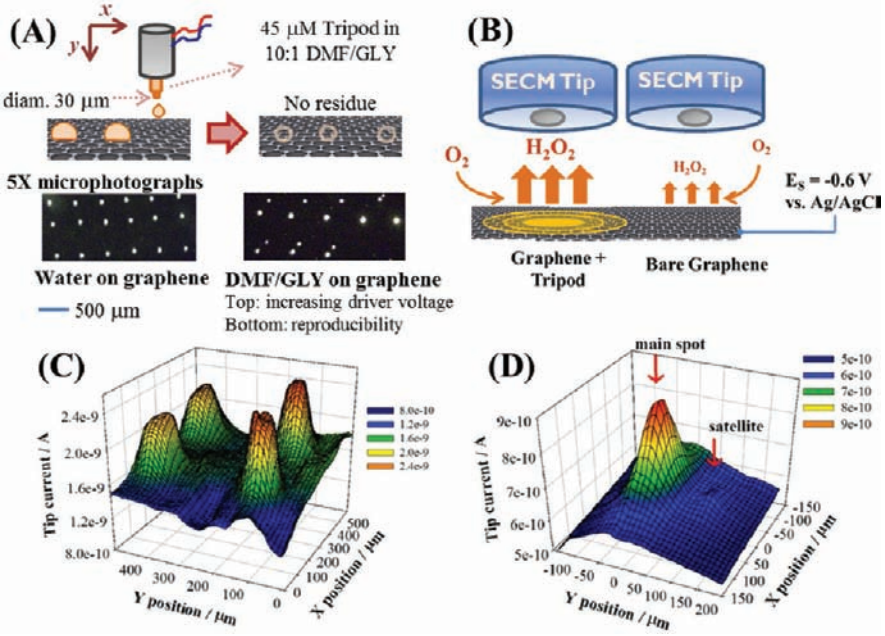


**Figure 5.** Tripod microspot deposition on graphene and HOPG. (A) Schematics of microdroplet deposition on the graphene surface from an organic precursor solution using a piezoelectric dispenser. Optical micrographs show satellite spots during droplet dispensing of DMF/GLY solutions that are not observed when aqueous solutions are deposited, but good reproducibility of overall size and shape in both cases. (B) Schematics of imaging tripod microspots by collecting $H_2O_2$ produced at the substrate during ORR. (C, D) SECM $H_2O_2$ substrate generation/tip collection experiments for (C) an array of **1·2PF$_6$** microspots (100 pmol/cm$^2$, $b$ = 50 $\mu$m) on HOPG (recorded at $t$ = 2 400 s) and (D) a **1·2PF$_6$** microspot (100 pmol/cm$^2$, $b$ = 50 $\mu$m) on SLG (recorded at $t$ = 6 300 s) that shows a satellite spot seen in panel A. For each experiment, $H_2O_2$ collection at the SECM tip ($a$ = 12.5 $\mu$m Pt, RG ≈ 7) was performed at $E_T$ = 0.6 V vs Ag/AgCl, interelectrode distance $d$ = 10 $\mu$m, and $E_S$ = −0.6 V vs Ag/AgCl.

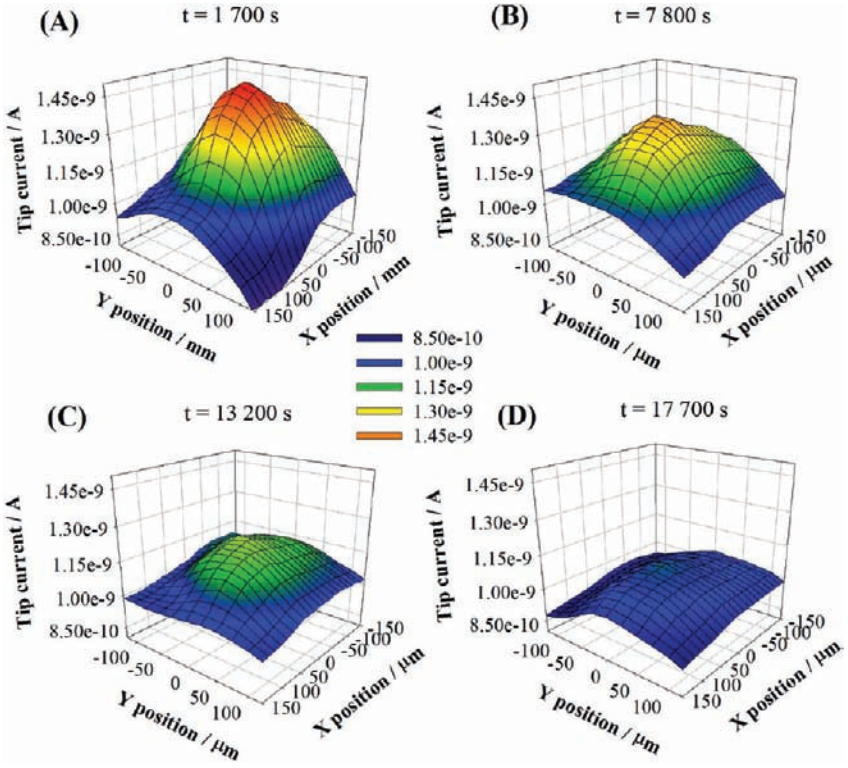


**Figure 6.** Progression of SECM hydrogen peroxide substrate generation/tip collection images for a representative **1·2PF$_6$** microspot on graphene (100 pmol/cm$^2$, $b$ = 50 $\mu$m). Images A–D were obtained at the indicated times. $H_2O_2$ collection at the SECM tip ($a$ = 12.5 $\mu$m Pt, RG ≈ 7) was performed at $E_T$ = 0.6 V vs Ag/AgCl, interelectrode distance $d$ = 10 $\mu$m, and $E_S$ = −0.6 V vs Ag/AgCl. The substrate potential $E_S$ was −0.6 V vs Ag/AgCl throughout the experiment.


dx.doi.org/10.1021/ja2106724 | J. Am. Chem. Soc. 2012, 134, 6224–6236

under similar conditions), which suggests kinetic control below this potential. Furthermore, a graphene microelectrode experiment designed to estimate the percentage of $H_2O_2$ output (Supporting Information Figure S5), i.e., the contribution of eq 1 to the ORR process,[74] over this potential region indicates that the total ORR current is less than 0.25 times the limiting current (assuming the limiting 4-electron route) at potentials more positive than $E_S$ = −0.6 V vs Ag/AgCl. Under these conditions, the $\%H_2O_2$ is less than ∼20% for bare graphene, while that of tripod-adsorbed graphene shows higher values of ∼40%. Under these kinetic limitations and although likely dominated by convection of $O_2$ toward the graphene substrate, a steady background suitable for imaging on a bare SLG electrode is obtained (Supporting Information Figure S6, $E_S$ = −0.6 V vs Ag/AgCl).

After establishing that adsorbed **1·2PF$_6$** presents a differential reactivity during the ORR on graphene, we employed a "microspot" approach to evaluate the mobility of the tripods on the SLG surface (Figure 1). A piezoelectric dispenser (Figure 5A) was used to deliver small droplets of a solution of **1·2PF$_6$** in DMF/GLY (10:1 *v*/*v*), forming an initial boundary with monolayer coverage of the species after solvent evaporation. The droplets form well-defined areas that were observed by optical microscopy. The ORR occurs on the entire substrate, yielding a background level of $H_2O_2$ collection (Figure 5B) over unfunctionalized regions of the electrode, as well as larger collection currents over areas where the tripod is adsorbed. Figure 5C shows an array of tripod microspots deposited on HOPG ($b$ = 50 and 300 $\mu$m center to center). The areas where tripod spots were deposited are clear, and their sizes correspond well to those observed by optical microscopy. Figure 5D shows a microspot on a SLG electrode, where a satellite spot, created by an irregular deposition from the dispenser, is also observed. The observation of these irregularities further confirms the ability of the SECM to detect **1·2PF$_6$** deposited on SLG. The spots in Figure 5C,D are also well below the maximum $H_2O_2$ collection observed for glassy carbon (Supporting Information Figures S4 and S7). Experiments in which blank solvent was deposited did not show any activity over the background.

We assume that the necessary conditions to allow mobility of **1·2PF$_6$** from its initial confinement toward the bulk graphene surface are present once the electrode is completely immersed in the electrolytic environment. The tip current observed due to collection of $H_2O_2$ over microspots of **1·2PF$_6$** on SLG decreases with time in a manner consistent with surface diffusion. Figure 6 and Supporting Information Figure S8 show a typical progression of this change in activity. It should be noted that an approximate background of ∼0.85 nA is present throughout the experiment even as the spot activity decreases, indicating that potential complications, such as fouling of the SECM tip, are unimportant (occasional cleaning of the tip was performed with similar results). The collection intensities observed for an approximate initial monolayer coverage of **1·2PF$_6$** and for the SLG background are well below that observed for blank glassy carbon, confirming that the requisite kinetic control for modeling surface diffusion response is followed at $E_S$ = −0.6 V vs Ag/AgCl. An approximate calibration of the $H_2O_2$ output in $b$ = 50 $\mu$m spots for selected initial surface concentrations is also shown in Supporting Information Figure S9 and indicates the decreasing trend in activity at lower surface concentrations. The time dependence of the collection intensity at the center of a microspot expected for surface diffusion, normalized to its initial intensity, was simulated with respect to the normalized time $\tau$ (Figure 7).

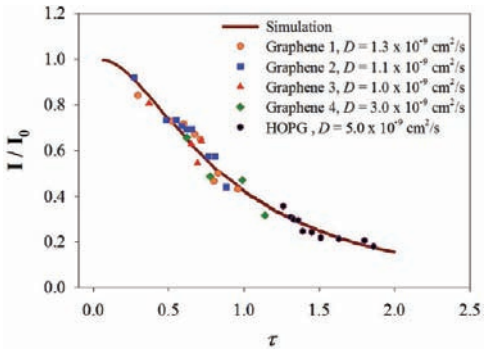


**Figure 7.** Comparison of simulation and experiment for $H_2O_2$ collection experiments performed over the center of **1·2PF$_6$** microspots ($r$ = 0). The experimental data were background subtracted and fitted to the simulation by choice of $D$ (implicit in $\tau$) as explained in the text. All conditions as in Figure 6.

This simulation is analogous to the concentration profile shown for the surface species in Figure 2 for $r$ = 0$b$ and also accounts for the contribution of the tip and substrate geometries to the electrochemical signal. Data from many **1·2PF$_6$** microspots were fit to this curve, and the experimental responses (after background subtraction to provide the changes in the peak intensities) were adjusted to the main curve by the choice of $D$ in the normalized time axis (eq 3).[98] An excellent agreement to the simulation was observed over the steep region of the curve ($\tau$ < 1). Averaging these data yields $D$ = 1.6 (±0.9) × $10^{-9}$ $cm^2/s$, a value fully consistent with surface diffusion. Differences between graphene substrates may occur because of heterogeneous distribution of defects, grain boundaries, and inconsistencies in transferring graphene to the $Si/SiO_2$ support (e.g., presence of nanometer-scale ripples). Nonetheless, all samples display surface diffusion values within the same order of magnitude.

A variety of control experiments support our interpretation of the above data as the diffusion of **1·2PF$_6$** on the SLG surface and preclude many plausible alternative explanations. Stirring the solution between experiments did not appreciably change the SECM response except for small changes in the graphene background current. This indicates that convective transport of the adsorbed tripod does not contribute significantly to the decrease in the activity of the microspots. In addition, an oxygen depletion effect cannot account for the observed decrease in the activity of the microspot, because the SECM was also open to air saturation throughout the experiment. We also confirmed that the SLG remains stable under the experimental conditions and potentials for long periods of time. For example, even at a higher overpotential ($E_S$ = −1.0 V vs Ag/AgCl) than was used above, an SLG microelectrode consisting of graphene surrounded by cured photoresist exhibits only a ± 2.5% current variation over a period of 8000 s (Supporting Information Figure S10). Next, we designed an experiment to interrupt the diffusion of **1·2PF$_6$** on the SLG surface. In this situation, no decrease of its electrochemical response over time would be expected. Figure 8A−D shows a progression of images of a **1·2PF$_6$** microspot on an SLG electrode treated with an electroactive thin layer of poly(vinylpyridine)/poly(vinylferrocene) (PVP/PVF) so as to disrupt the mobility of the tripod on the surface without


dx.doi.org/10.1021/ja2106724 | J. Am. Chem. Soc. 2012, 134, 6224−6236

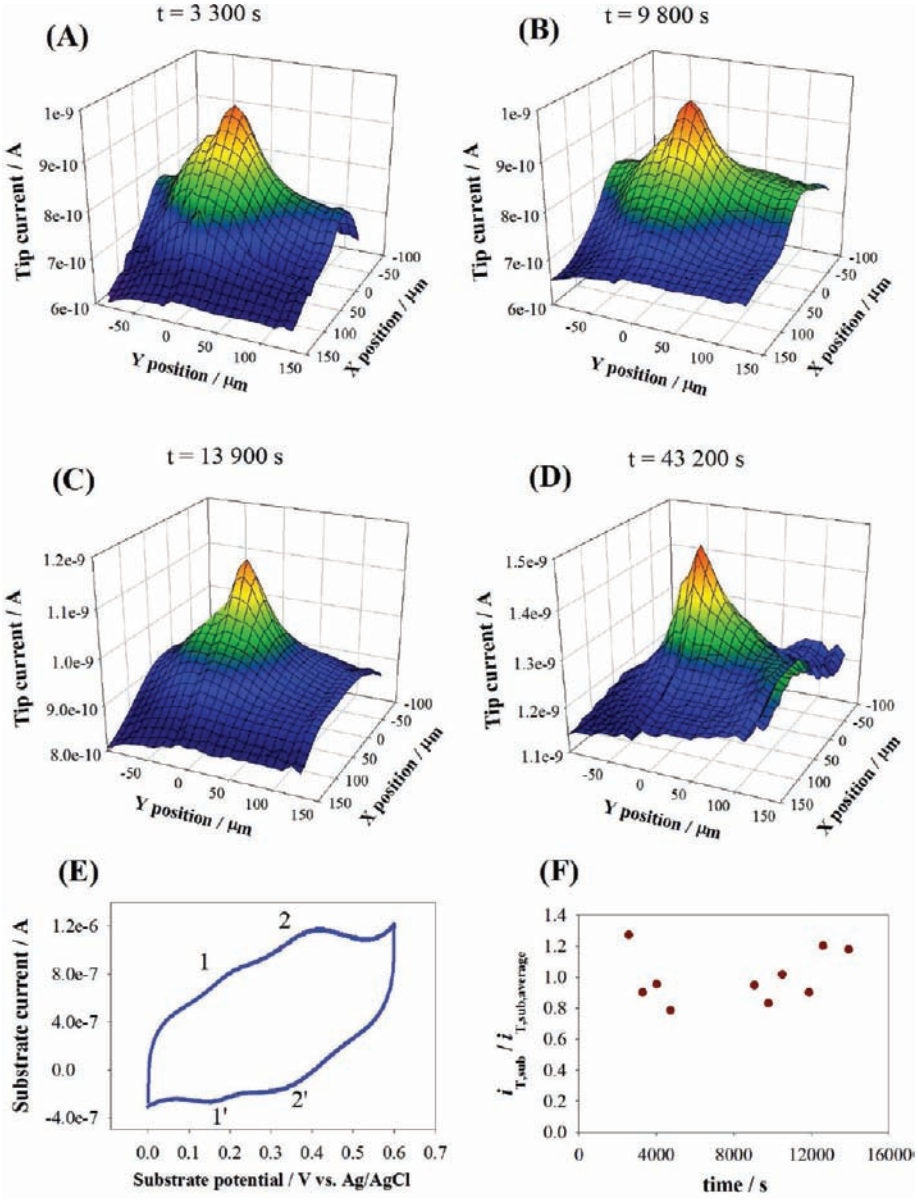


**Figure 8.** Representative SECM $H_2O_2$ substrate generation/tip collection images for a **1·2PF$_6$** microspot (~100 pmol/cm$^2$, $b \approx 40$ $\mu$m) on a surface-disrupted SLG electrode. The graphene was pretreated with a 0.1 mg/mL ethanolic solution of PVP/PVF copolymer 2:1 to a final coverage of ~90 pmol/cm$^2$ of ferrocene redox centers. Images A–D were obtained at the indicated times. $H_2O_2$ collection at the SECM tip ($a$ = 12.5 $\mu$m Pt, RG ≈ 7) was performed at $E_T$ = 0.6 V vs Ag/AgCl, interelectrode distance $d$ = 10 $\mu$m, and $E_S$ = −0.6 V vs Ag/AgCl. The surface potential was held at $E_S$ throughout the experiment except for image D. (E) Cyclic voltammogram showing adsorption of PVP/PVF and tripod spots (from the entire array), $\nu$ = 100 mV/s. (F) Plot of background subtracted collection currents, normalized to the average measured current vs time (<16,000 s).

damaging the SLG. The presence of the polymer is confirmed by its electrochemical response (Figure 8E, process 2 and 2′), in addition to the **1·2PF$_6$** signal (process 1 and 1′). Although $H_2O_2$ collection measurements over a **1·2PF$_6$** microspot show some variability in their electrochemical response over 43,000 s (Figure 8F), no clear decreasing trend in activity is observed, in contrast to the continuous decrease in activity of the microspots observed in the absence of the PVP/PVF diffusion barrier (compare to Figure 7). The presence of the co-adsorbed PVP/PVF polymer introduces a physical barrier ~5–10 nm high over lengths of hundreds of micrometers (Supporting Information Figure S11) where **1·2PF$_6$** is unlikely to traverse or displace the adsorbed polymeric units. This prevents mass transfer diffusion of **1·2PF$_6$** out of its initial confinement, although individual molecules may still preserve mobility within much smaller domains. Taken together, the above control experiments strongly suggest that surface diffusion is the main mechanism for the observed decrease in the analytical signal of **1·2PF$_6$** microspots on SLG.

**Feedback Experiments.** The $H_2O_2$ collection experiments described above measure the activity of the underlying surface indirectly by detecting the product of an electrocatalytic reaction at the SECM tip. We also probed the activity of **1·2PF$_6$** at the SLG surface more directly using the feedback mode of SECM (Figure 9A). In this experiment, a dissolved redox mediator is used to continuously generate, at steady state, a reactive species at the SECM tip. The tip is moved toward the surface to a distance comparable to that of its active microdisk (described by the normalized distance $L = d/a$ where $d$ is the tip–substrate distance), and the reactive form of the mediator


dx.doi.org/10.1021/ja2106724 | J. Am. Chem. Soc. 2012, 134, 6224–6236

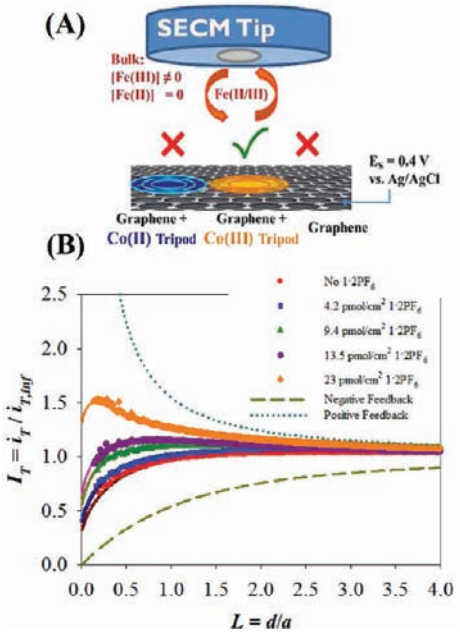


**Figure 9.** Use of SECM feedback for the detection of adsorbed, activated Co(III) tripod at graphene using a Fe(II/III) mediator couple. (A) Schematic of the use of SECM feedback to detect the Co(III) oxidation state of the tripodal compound adsorbed on graphene. The reduced Fe(II) complex reacts more quickly with the Co(III) tripod than the unfunctionalized SLG substrate. (B) Approach curves on HOPG with increasing coverages of adsorbed **1·2PF$_6$** (as indicated) in a potassium ferricyanide (1.65 mM) phosphate buffer solution (0.2 M, pH 7); $E_S$ = 0.4 V vs Ag/AgCl, $E_T$ = −0.1 V vs Ag/AgCl. The SECM tip had $a$ = 12.5 $\mu$m Pt with RG ≈ 7. Solid lines based on theory for heterogeneous kinetics (rates shown in Supplementary Figure S12).

diffuses to the substrate, which is typically biased to a potential where it can perform the reverse of the reaction occurring at the tip.[33] For example, if the SECM tip reduces the soluble redox mediator, the mediator is regenerated by oxidation at the bulk substrate electrode. For typical conductive substrates, such as metal electrodes and glassy carbon, most electrochemically reversible mediators react rapidly at the surface. In this situation, the current read at the SECM tip increases at distances $L$ < 1 because the mass transfer coefficient of the redox mediator increases as the tip−substrate separation decreases, a phenomenon known as positive feedback. In contrast, an insulating or inactive surface causes the tip current to decrease as the tip approaches the surface, a negative feedback effect. Furthermore, the kinetics of electron transfer between the electrodes and the redox mediator may be evaluated within the context of these two feedback regimes. Although SLG is highly conductive over its basal plane, its rate of interfacial charge transfer to the Fe(II/III) complex ferro/ferricyanide is expected to be similar to that of HOPG. Adsorbed **1·2PF$_6$** increases the electrochemical activity of the SLG electrode (see below), and this differential reactivity between functionalized and nonfunctionalized SLG provides contrast in the SECM measurement that allows the surface diffusion of the tripodal binding motif to be measured.

Figure 9B shows approach curves (i.e., steady-state current vs $L$ curves, from which the value of the heterogeneous charge transfer rate constant can be extracted) generated using the ferri/ferrocyanide $Fe(CN)_6^{3-/4-}$ couple ($E^0$ = 0.16 V vs Ag/AgCl) as the soluble redox mediator and an HOPG bulk electrode at a constant $E_S$ = 0.4 V vs Ag/AgCl. Under these conditions noble metal substrates (e.g., Pt, Au) would show almost complete positive feedback, but the approach curve for the unfunctionalized HOPG electrode (Figure 9B, red) indicates negative feedback-like behavior with a small yet measurable charge transfer rate constant. The slow rate of electron transfer between ferri/ferrocyanide and HOPG electrodes is well-known[17,18] and is attributable to the low density of states on the material relative to metallic electrodes,[99] effects of the self-exchange rate constants of the mediator,[89] and effects of oxygenated defects.[90] The approach curves for HOPG electrodes functionalized with **1·2PF$_6$** show a clear increase in the rate of charge transfer for the ferrocyanide mediator (Figure 9B), as reflected by the higher currents observed at smaller tip/sample distances ($L$) and by their characteristic shape in this intermediate kinetic regime. A linear relationship between the heterogeneous electron transfer rate constant and the tripod surface concentration (Supporting Information Figure S12) was observed, corresponding to a second order electron transfer rate constant $k_{ex}$ = 1.6 × $10^8$ $mol^{-1}$ $cm^3$ $s^{-1}$ between the Co(III) tripod and $Fe(CN)_6^{4-}$. Although higher exchange rate constants have been observed for highly electrochemically reversible systems (~$10^{10}$ $mol^{-1}$ $cm^3$ $s^{-1}$),[84] this value is similar to that measured for electron transfer between the iron active site of cytochrome c and ferricyanide ($k_{ex}$ = 2 × $10^8$ $mol^{-1}$ $cm^3$ $s^{-1}$)[85] and exceeds that of complex oxide reduction mechanisms involving additional proton transfers ($k_{ex}$ < 1 × $10^8$ $mol^{-1}$ $cm^3$ $s^{-1}$).[91] It is also likely that the relatively low $k_{ex}$ value also reflects the low self-exchange rate constant for Co(II/III) terpyridine and bipyridine couples.[70−73] Nevertheless, the increased electrochemical activity of the bulk electrode upon adsorption of **1·2PF$_6$** provides a means to characterize molecular diffusion by measuring the time dependence of the feedback current obtained over **1·2PF$_6$** microspots.

Figure 10 shows a progression of feedback images for a **1·2PF$_6$** microspot ($b$ ≈ 15 $\mu$m) deposited on graphene with the substrate potential held at $E_S$ = 0.4 V vs Ag/AgCl and interrogated using tip generated $Fe(CN)_6^{4-}$ in phosphate buffer. A decrease in the peak intensity of the feedback current with respect to time was observed, similar to the trend observed in the $H_2O_2$ collection experiments. A small increase in the electrochemical activity of the surrounding SLG was also observed over the course of the experiment. We attribute this increase to the diffusion of **1·2PF$_6$** from the microspots into the surrounding unfunctionalized area of the SLG, although it is difficult to deconvolve this small change from other sources of background drift. We also observed similar behavior at a larger microspot (Supporting Information Figure S13) and performed control experiments to support our interpretation of the feedback measurments. First, images obtained at open circuit (Supporting Information Figure S13), at which the Co(III) species is not deliberately formed on the SLG surface, show almost no difference in the feedback current as compared to unfunctionalized graphene. The stability of the SLG electrode at oxidizing potentials was also confirmed by measuring the average collection current associated with generating the hydroxymethylferricenium ion ($E_S$ = 0.4 V vs Ag/AgCl) over a period of 6,000 s. These collection currents varied up to ±8%, but no degrading trend for the electrode was observed (Supporting Information Figure S14). Furthermore, no significant formation of oxygenated defects on the SLG is expected at the potentials used for these measurements.[22] It


dx.doi.org/10.1021/ja2106724 | J. Am. Chem. Soc. 2012, 134, 6224−6236

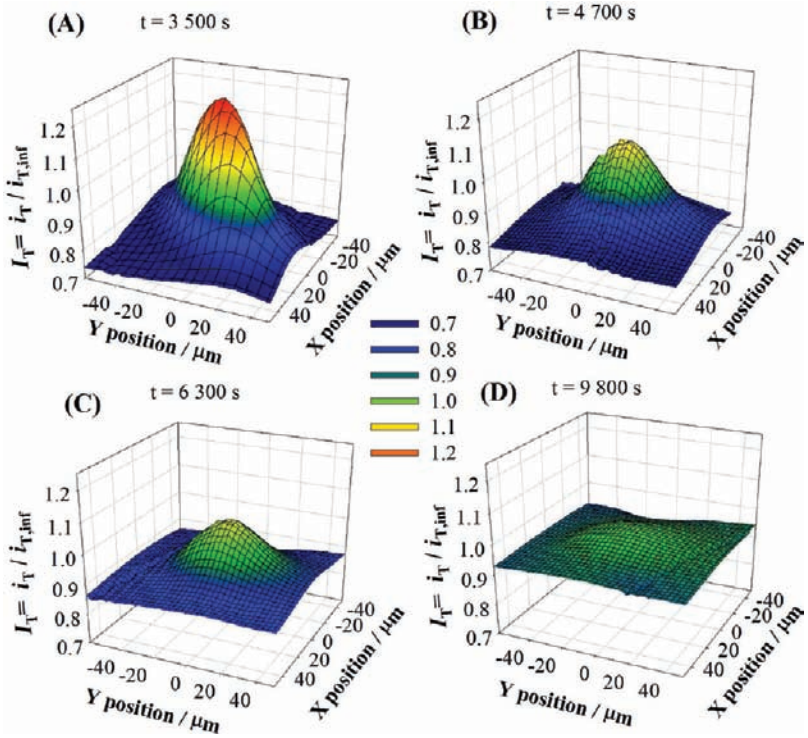


**Figure 10.** Progression of SECM feedback images for a representative **1·2PF$_6$** microspot (~140 pmol/cm$^2$, $b$ = 15 $\mu$m) on SLG. The experiment used a potassium ferricyanide mediator (2 mM) in phosphate buffer (0.2 M, pH = 7). Images A–D were obtained at the indicated times. The SECM tip was $a$ = 12.5 $\mu$m Pt, RG ≈ 7 with an interelectrode distance $d$ = 10 $\mu$m. Feedback was carried out at $E_T$ = −0.1 V vs Ag/AgCl and $E_S$ = 0.4 V vs Ag/AgCl. The substrate potential was held at $E_S$ throughout the experiment.

was also possible to detect the **1·2PF$_6$** microspots using other Fe redox mediators, such as FeEDTA ($E^0$ = −0.08 V vs Ag/AgCl, Supporting Information Figure S15). The use of Fe(II/III)EDTA was not pursued further because it would require that these time-sensitive measurements be performed in an inert atmosphere.

The peak feedback currents measured at the center of the microspot were fit to a diffusion model (Figure 11) whose

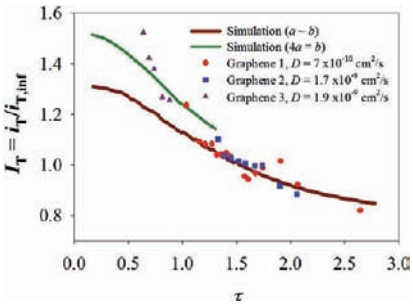


**Figure 11.** Comparison of simulation and experiment for ferrocyanide feedback experiments performed over the center of **1·2PF$_6$** microspots (140 pmol/cm$^2$, $r$ = 0). The experimental data were fitted to simulation by the choice of $D$ (implicit in $\tau$) as explained in the text. Conditions as in Figure 10. The simulations assume a Co(III)-ferrocyanide exchange constant $k_{ex}$ of 1.6 × 10$^8$ mol/cm$^3$s and an SLG background constant $k_{back}$ of 0.8 × 10$^{-3}$ cm/s. The simulated $D$ for ferri/ferrocyanide was 7.2 × 10$^{-6}$ cm$^2$/s for both forms of the redox pair. Two sets of data are shown, one for microspots $b$ ≈ 15 $\mu$m (red circles and blue squares) and another for $b$ ≈ 50 $\mu$m. (purple triangles). The first point of each experimental series was obtained at a higher tip scan rate (see Experimental Section) and may reflect some advective effects.

input parameters included the measured exchange rate between the adsorbed Co(III) complex and Fe(CN)$_6^{4-}$, the initial surface concentration of **1·2PF$_6$**, and the charge transfer rate constant of the unfunctionalized SLG electrode (see Supporting Information). Two microspot sizes (15 and 50 $\mu$m diameter) were analyzed to confirm the model's applicability. The diffusion coefficient obtained by fitting the absolute feedback measurements ($D_{eff}$ = 1.5 (±0.6) × 10$^{-9}$ cm$^2$/s) is in good agreement with that derived from the $H_2O_2$ collection measurements ($D_{eff}$ = 1.6 (±0.9) × 10$^{-9}$ cm$^2$/s). Finally, the improved lateral resolution of feedback measurements enabled further inspection of the electrochemical response of the SLG surface away from the center of the **1·2PF$_6$** microspots, which provide further qualitative confirmation of our surface diffusion model. We compared the results of three-dimensional simulations (Supporting Information Figure S16), in which a nonuniform surface concentration profile is translated into a tip response, to the experimental lateral tip currents from the experiment shown in Figure 10. A reasonable agreement between simulation and experiment was obtained, which reproduces the concurrent decrease of the peak response, close to the center of the microspot, and increased response in the surrounding graphene material associated with diffusion of the tripods from the microspots. Although the SECM tip size is not necessarily optimal for this analysis, these simulations do confirm that the broadening of the signal at longer times is a much less sensitive measure of diffusion than the decrease in the peak intensity of the microspot (see above).

The similarity of the surface diffusion values obtained from either G/C or feedback measurements is remarkable, considering the fundamental mechanistic differences, as well as the ~1 V difference in substrate potential, associated with


dx.doi.org/10.1021/ja2106724 | J. Am. Chem. Soc. 2012, 134, 6224–6236

the two experiments. The potential of zero charge (PZC) of the basal plane of HOPG has been reported[89] to be ~ −0.2 V vs Ag/AgCl and recent charge carrier measurements on solution-gated graphene field effect transistors show a minimum conductivity, carrier concentration, and shift in carrier entity at ~ −0.4 V vs Ag/AgCl,[14] which might be closely related to the PZC of graphene. The substrate potentials employed in our studies lie on either side of these values, suggesting that the diffusion of the tripodal binding motif is relatively insensitive to excess charge from adsorbed ions at the graphene/solution interface. Thus, the rate of tripod diffusion might instead be limited by solvent displacement processes or by decreased mobility at graphene defects and edges. The description of these effects lies outside the scope of this manuscript, but their further study is relevant for designing new mobile adsorbates on SLG and other technologically relevant surfaces.

This study represents a macroscopic approach to measuring the diffusion coefficient of the tripodal compounds on SLG and provides an effective value that applies over large distances and times, similar to those obtained by fluorescence in FRAP experiments. These values are distinct from those obtained through single molecule experiments.[49] We have not yet considered the effects of the surface roughness on the response. Scanning probe experiments have found that graphene transferred onto $SiO_2$ partially adapts to the morphology of the underlying substrate,[100] with root-mean-square roughness of ~3 nm over 100 $\mu m^2$. This roughness is approximately three to four times the graphene layer thickness of 0.8 nm[101] and is less pronounced in high-quality HOPG.[102] This difference in surface roughness is one explanation for the larger surface diffusion coefficient for HOPG shown in Figure 7. Reduced diffusion along defects and grain boundaries in our SLG samples[103] may also reduce the measured effective diffusion coefficients. However, it has been observed that favorable $\pi$-stacking interactions are relatively insensitive to these features, including steps in single to bilayer graphene.[43] **1·2PF$_6$** is designed to adsorb onto the pristine $sp^2$ surface of graphene, unlike other aromatic molecules that prefer adsorption at defects on HOPG.[104] However, we cannot discount that favorable interactions between defects and the tripod could account for slowing down its surface mobility. The value obtained here is also at least 3 orders of magnitude lower than that computationally predicted in vacuum for adsorbed aromatics,[105,106] although this discrepancy can be explained by the lack of description of ion and solvent displacement in such theoretical treatments. Intuitively, the obtained value fits well a middle region between diffusion in solution and in solids.

## CONCLUSIONS

Scanning electrochemical microscopy was used to detect the activity and quantify the surface diffusion of tripodal compound **1·2PF$_6$** adsorbed onto SLG and the basal plane of HOPG using two complementary methods. The first method used the substrate generation/tip collection (G/C) mode of SECM to exploit the electrocatalytic properties of the adsorbed tripod, which produced larger amounts of $H_2O_2$ than the bare graphene surface in the oxygen reduction reaction. A second method used the feedback mode, in which the tripod mediates the oxidation of ferrocyanide produced at the tip faster than the bare graphene electrode. For each measurement, the increased electrochemical activity of the adsorbed molecules relative to the SLG electrode provided sufficient contrast to image microspots of the tripodal molecules with spatial and temporal resolution. We attribute the decreased electrochemical response of the tripodal microspots over time to diffusion of the molecules onto the unfunctionalized regions of the SLG electrode. A framework for describing this diffusion in terms of the decrease of the peak intensity of the microspots due to radial dilution, as detected by SECM, was successfully implemented. The two imaging strategies yielded similar values of the macroscopic surface diffusion ($D_{eff}$) of the tripod on the graphene surface: $D_{eff}$ = 1.6 (±0.9) × $10^{-9}$ $cm^2/s$ at $E_S$ = −0.6 V vs Ag/AgCl and $D_{eff}$ = 1.5 (±0.6) × $10^{-9}$ $cm^2/s$ at $E_S$ = 0.4 V vs Ag/AgCl for G/C and feedback modes, respectively. Control experiments, in which the stability of graphene was tested, as well as experiments in which the mobility of the tripodal molecules was disrupted by coadsorption of a polymer, strongly support our surface diffusion hypothesis.

The development of an SECM-based technique for quantifying molecular surface diffusion on electrodes, specifically on graphene as a model carbon surface, is an important addition to the understanding and control of molecular electrocatalysis for sensing and energy conversion systems. It also presents interesting possibilities in the field of molecular electronics, where the coupling of the unique electronic and mechanical properties of graphene together with its surface mass transfer properties can now be studied and quantitatively described. Our laboratory is currently working to image graphene using SECM at higher resolution in order to describe this material and its interactions in better detail. For instance, we hope to explore the impact of grain boundaries, single crystallites (ranging from a few to tens of micrometers), reactive defects, and heteroatom substitutions on the electrochemical reactivity of this promising material.

## ASSOCIATED CONTENT

### Supporting Information

Experimental details of graphene growth, supporting experiments for the characterization of **1·2PF$_6$** activity, and a complete description of the simulation model. This material is available free of charge via the Internet at http://pubs.acs.org.

## AUTHOR INFORMATION

### Corresponding Author

wdichtel@cornell.edu; hda1@cornell.edu

### Notes

The authors declare no competing financial interest.

## ACKNOWLEDGMENTS

The authors acknowledge NSF CCI-phase I (0847926) for financial support. The authors thank CNF (ECS 0335765) and CCMR (DMR 1120296) for providing fabrication facilities and instrumentation; Professor Paul L. McEuen, Professor Jiwoong Park, and Kevek Innovations for help with graphene growth; and Dr. Eric Rus for helpful discussions. N.L.R., C.T., and J.A.M. gratefully acknowledge the Integrative Graduate Education and Research Traineeship (IGERT) Program in the Nanoscale Control of Surfaces and Interfaces, which is supported under NSF Award DGE-0654193, the Cornell Center for Materials Research, and Cornell University.

## REFERENCES

(1) Novoselov, K. S.; Geim, A. K.; Morozov, S. V.; Jiang, D.; Zhang, Y.; Dubonos, S. V.; Crigorieva, I. V.; Firsov, A. A. *Science* **2004**, *306*, 666−669.

(2) Stankovich, S.; Dikin, D. A.; Dommett, G. H. B.; Kohlhaas, K. M.; Zimney, E. J.; Stach, E. A.; Piner, R. D.; Nguyen, S. T.; Ruoff, R. S. *Nature* **2006**, *442*, 282−286.
(3) Geim, A. K.; Novoselov, K. S. *Nat. Mater.* **2007**, *6*, 183−191.
(4) Geim, A. K. *Science* **2009**, *324*, 1530−1534.
(5) Li, W.; Tan, C.; Lowe, M. A.; Ralph, D. C.; Abruña, H. D. *ACS Nano* **2011**, *5*, 2264−2270.
(6) Wang, X.; Zhi, L.; Müllen, K. *Nano Lett.* **2007**, *8*, 323−327.
(7) Kumar, A.; Zhou, C. *ACS Nano* **2010**, *4*, 11−14.
(8) Li, X.; Zhu, Y.; Cai, W.; Borysiak, M.; Han, B.; Chen, D.; Piner, R. D.; Colombo, L.; Ruoff, R. S. *Nano Lett.* **2009**, *9*, 4359−4369.
(9) Bunch, J. S.; van der Zande, A. M.; Verbridge, S. S.; Frank, I. W.; Tanenbaum, D. M.; Parpia, J. M.; Craighead, H. G.; McEuen, P. L. *Science* **2007**, *315*, 490−493.
(10) Van der Zande, A. M.; Barton, R. A.; Alden, J. S.; Ruiz-Vargas, C. S.; Whitney, W. S.; Pham, P.H.-Q.; Park, J.-W.; Parpia, J. M.; Craighead, H. G.; McEuen, P. L. *Nano Lett.* **2010**, *10*, 4869−4873.
(11) Lee, W. H.; Park, J.; Sim, S. H.; Lim, S.; Kim, K. S.; Hong, B. H.; Cho, K. *J. Am. Chem. Soc.* **2011**, *133*, 4447−4454.
(12) Liu, W.; Jackson, B. L.; Zhu, J.; Miao, C.-Q.; Chung, C.-H.; Park, Y. J.; Sun, K.; Woo, J.; Xie, Y.-H. *ACS Nano* **2010**, *4*, 3927−3932.
(13) Jang, S.; Jang, H.; Lee, Y.; Suh, D.; Baik, S.; Hong, B. H.; Ahn, J.-H. *Nanotechnology* **2010**, *21*, 425201/1−425201/5.
(14) Dankerl, M.; Hauf, M. V.; Lippert, A.; Hess, L. H.; Birner, S.; Sharp, I. D.; Mahmood, A.; Mallet, P.; Veuillen, J.-Y.; Stutzmann, M.; Garrido, J. A. *Adv. Funct. Mater.* **2010**, *20*, 3117−3124.
(15) Cheng, H.-C.; Shiue, R.-J.; Tsai, C.-C.; Wang, W.-H.; Chen, Y.-T. *ACS Nano* **2011**, *5*, 2051−2059.
(16) Coletti, C.; Riedl, C.; Lee, D. S.; Krauss, B.; Patthey, L.; von Klitzing, K.; Smet, J. H.; Starke, U. *Phys. Rev. B* **2010**, *81*, 235401/1−235401/8.
(17) McCreery, R. L. *Chem. Rev.* **2008**, *108*, 2646−2687.
(18) McCreery, R. L. Carbon Electrodes: Structural Effects on Electron Transfer Kinetics. In *Electroanalytical Chemistry*; Bard, A. J., Ed.; Marcel Dekker: New York, 1991; Vol.*17*, pp 221−374.
(19) Edwards, M. A.; Bertoncello, P.; Unwin, P. R. *J. Phys. Chem. C* **2009**, *113*, 9218−9223.
(20) Dumitrescu, I.; Dudin, P. V.; Edgeworth, J. P.; Macpherson, J. V.; Unwin, P. R. *J. Phys. Chem. C* **2010**, *114*, 2633−2639.
(21) Heller, I.; Kong, J.; Heering, H. A.; Williams, K. A.; Lemay, S. G.; Dekker, C. *Nano Lett.* **2005**, *5*, 137−142.
(22) Lim, C. X.; Hoh, H. Y.; Ang, P. K.; Loh, K. P. *Anal. Chem.* **2010**, *82*, 7387−7393.
(23) Qu, L.; Liu, Y.; Baek, J.-B.; Dai, L. *ACS Nano* **2010**, *4*, 1321−1326.
(24) Scida, K.; Stege, P. W.; Haby, G.; Messina, G. A.; Garcia, C. D. *Anal. Chim. Acta* **2011**, *691*, 6−17.
(25) Ratinac, K. R.; Yang, W.; Gooding, J. J.; Thordarson, P.; Braet, F. *Electroanalysis* **2011**, *23*, 803−826.
(26) Pumera, M. *Chem. Rec.* **2009**, *9*, 211−223.
(27) Brownson, D. A. C.; Banks, C. E. *Analyst* **2010**, *135*, 2768−2778.
(28) Hasin, P.; Alpuche-Avilés, M. A.; Wu, Y. *J. Phys. Chem. C* **2010**, *114*, 15857−15861.
(29) Shao, Y.; Wang, Y.; Wu, H.; Liu, J.; Aksay, I. A.; Lin, Y. *Electroanalysis* **2010**, *22*, 1027−1036.
(30) Mann, J. A.; Rodríguez-López, J.; Abruña, H. D.; Dichtel, W. R. *J. Am. Chem. Soc.* **2011**, *133*, 17614−17617.
(31) Tasis, D.; Tagmatarchis, N.; Bianco, A.; Prato, M. *Chem. Rev.* **2006**, *106*, 1105−1136.
(32) *Scanning Electrochemical Microscopy*; Bard, A. J., Mirkin, M. V., Eds.; Marcel Dekker: New York, 2001.
(33) Bard, A. J.; Fan, F.-R. F.; Mirkin, M. V. Scanning Electrochemical Microscopy. In *Electroanalytical Chemistry*; Bard, A. J., Ed.; Marcel Dekker: New York, 1993, Vol. *18*, pp 243−373.
(34) Bard, A. J.; Denuault, G.; Lee, C.; Mandler, D.; Wipf, D. O. *Acc. Chem. Res.* **1990**, *23*, 357−363.
(35) Savéant, J.-M. *Chem. Rev.* **2008**, *108*, 2348−2378.
(36) McCrory, C. C. L.; Devadoss, A.; Ottenwaelder, X.; Lowe, R. D.; Stack, D. P.; Chidsey, C. E. D. *J. Am. Chem. Soc.* **2011**, *133*, 3696−3699.
(37) Park, J.; Pasupathy, N.; Goldsmith, J. I.; Chang, C.; Yaish, Y.; Petta, J. R.; Rinkoski, M.; Sethna, J. P.; Abruña, H. D.; McEuen, P. L.; Ralph, D. C. *Nature* **2002**, *417*, 722−725.
(38) Metzger, R. M. *J. Mater. Chem.* **2008**, *18*, 4364−4396.
(39) Marek Szklarczyk, M.; Strawski, M.; Bieńkowski, K. 25 years of the Scanning Tunneling Microscopy − 20 Years of Application of STM in Electrochemistry. In *Modern Aspects of Electrochemistry*; Vayenas, C. G.; White, R. E.; Gamboa-Aldeco, M. E., Eds.; Springer: New York, 2008; Vol. *42*, pp 303−368.
(40) Wang, D.; Wan, L.-J. *J. Phys. Chem. C* **2007**, *111*, 16109−16130.
(41) Kolb, D. M. *Angew. Chem., Int. Ed.* **2001**, *40*, 1162−1181.
(42) Itaya, K. *Prog. Surf. Sci.* **1998**, *58*, 121−248.
(43) Emery, J. D.; Wang, Q. H.; Zarrouati, M.; Fenter, P.; Hersam, M. C.; Bedzyk, M. J. *Surf. Sci.* **2011**, *605*, 1685−1693.
(44) Wang, Q. H.; Hersam, M. C. *Nat. Chem.* **2009**, *1*, 206−211.
(45) Kornberg, R. D.; McConnell, H. M. *Proc. Natl. Acad. Sci. U.S.A.* **1971**, *68*, 2564−2568.
(46) Köchy, T.; Bayerl, T. M. *Phys. Rev. E* **1993**, *47*, 2109−2116.
(47) Kobayashi, T.; Babu, P. K.; Gancs, L.; Chung, J. H.; Oldfield, E.; Wieckowski, A. *J. Am. Chem. Soc.* **2005**, *127*, 14164−14165.
(48) Tong, Y. Y.; Oldfield, E.; Wieckowski, A. *Faraday Discuss.* **2002**, *121*, 323−330.
(49) Sigaut, L.; Ponce, M. L.; Colman-Lerner, A.; Ponce Dawson, S. *Phys. Rev. E* **2010**, *82*, 051912.
(50) Naito, K.; Tachikawa, T.; Fujitsuka, M.; Majima, T. *J. Phys. Chem. C* **2008**, *112*, 1048−1059.
(51) Reits, E. A.J.; Neefjes, J. J. *Nat. Cell Biol.* **2001**, *3*, E145−E147.
(52) Axelrod, D.; Koppel, D. E.; Schlessinger, J.; Elson, E.; Webb, W. W. *Biophys. J.* **1976**, *16*, 1055−1067.
(53) Lorén, N.; Nydén, M.; Hermansson, A.-M. *Adv. Colloid Interface Sci.* **2009**, *150*, 5−15.
(54) Lu, C.-H.; Yang, H.-H.; Zhu, C.-L.; Chen, X.; Chen, G.-N. *Angew. Chem., Int. Ed.* **2009**, *48*, 4785−4787.
(55) Ramakrishna Matte, H. S. S.; Subrahmanyam, K. S.; Rao, K. V.; George, S. J.; Rao, C. N. R. *Chem. Phys. Lett.* **2011**, *506*, 260−264.
(56) Kim, J.; Cote, L. J.; Kim, F.; Huang, J. *J. Am. Chem. Soc.* **2010**, *132*, 260−267.
(57) He, S.; Song, B.; Li, D.; Zhu, C.; Qi, W.; Wen, Y.; Wang, L.; Song, S.; Fang, H.; Fan, C. *Adv. Funct. Mater.* **2010**, *20*, 453−459.
(58) Chen, Z.; Berciaud, S.; Nuckolls, C.; Heinz, T. F.; Brus, L. *ACS Nano* **2010**, *4*, 2964−2968.
(59) Unwin, P. R.; Bard, A. J. *J. Phys. Chem.* **1992**, *96*, 5035−5045.
(60) Slevin, C. J.; Unwin, P. R. *J. Am. Chem. Soc.* **2000**, *122*, 2597−2602.
(61) Zhang, J.; Unwin, P. R. *J. Am. Chem. Soc.* **2002**, *124*, 2379.
(62) Zhang, J.; Slevin, C.; Morton, C.; Scott, P.; Walton, D. J.; Unwin, P. R. *J. Phys. Chem. B* **2001**, *105*, 11120−11130.
(63) Zhang, J.; Unwin, P. R. *Phys. Chem. Chem. Phys.* **2002**, *4*, 3814−3819.
(64) O'Mullane, A. P.; Macpherson, J. V.; Unwin, P. R.; Cervera-Montesinos, J.; Manzanares, J. A.; Frehill, F.; Vos, J. G. *J. Phys. Chem. B* **2004**, *108*, 7219−7227.
(65) Mandler, D.; Unwin, P. R. *J. Phys. Chem. B* **2003**, *107*, 407−410.
(66) Bertoncello, P.; Ciani, I.; Li, F.; Unwin, P. R. *Langmuir* **2006**, *22*, 10380−10388.
(67) Whitworth, A. L.; Mandler, D.; Unwin, P. R. *Phys. Chem. Chem. Phys.* **2005**, *7*, 356−365.
(68) Zhang, J.; Barker, A. L.; Mandler, D.; Unwin, P. R. *J. Am. Chem. Soc.* **2003**, *125*, 9312−9313.
(69) Charych, D. H.; Landau, E. M.; Majda, M. *J. Am. Chem. Soc.* **1991**, *113*, 3340−3346.
(70) Takada, K.; Storrier, G. D.; Goldsmith, J. I.; Abruña, H. D. *J. Phys. Chem. B* **2001**, *105*, 2404−2411.
(71) Buttry, D. A.; Anson, F. C. *J. Am. Chem. Soc.* **1983**, *105*, 685−689.
(72) Farina, R.; Wilkins, R. G. *Inorg. Chem.* **1968**, *7*, 514−518.

(73) Chow, H. S.; Constable, E. C.; Housecroft, C. E.; Kulicke, K. J.; Tao, Y. *Dalton Trans.* **2005**, 236−237.
(74) Sanchez-Sanchez, C. M.; Rodriguez-Lopez, J.; Bard, A. J. *Anal. Chem.* **2008**, *80*, 3254−3260.
(75) Yeager, E. *Electrochim. Acta* **1984**, *29*, 1527−1537.
(76) Durand, R. R.; Anson, F. C. *J. Electroanal. Chem.* **1982**, *134*, 273−289.
(77) Horrocks, B. R.; Schmidtke, D.; Heller, A.; Bard, A. J. *Anal. Chem.* **1993**, *65*, 3605−3614.
(78) Wittstock, G.; Schuhmann, W. *Anal. Chem.* **1997**, *69*, 5059−5066.
(79) Ge, F.; Tenent, R. C.; Wipf, D. O. *Anal. Sci.* **2001**, *17*, 27−35.
(80) Wittstock, G.; Wilhelm, T. *Anal. Sci.* **2002**, *18*, 1199−1204.
(81) Sanchez-Sanchez, C. M.; Bard, A. J. *Anal. Chem.* **2009**, *81*, 8094−8100.
(82) Eckhard, K.; Schuhmann, W. *Electrochim. Acta* **2007**, *53*, 1164−1169.
(83) Pust, S. E.; Maier, W.; Wittstock, G. *Z. Phys. Chem.* **2008**, *222*, 1463−1517.
(84) Liu, B.; Bard, A. J.; Mirkin, M. V.; Creager, S. E. *J. Am. Chem. Soc.* **2004**, *126*, 1485−1492.
(85) Holt, K. B. *Langmuir* **2006**, *22*, 4298−4304.
(86) Wain, A. J.; Zhou, F. *Langmuir* **2008**, *24*, 5155−5160.
(87) Tefashe, U. M.; Loewenstein, T.; Miura, H.; Schlettwein, D.; Wittstock, G. *J. Electroanal. Chem.* **2010**, *650*, 24−30.
(88) Liu, B.; Rotenberg, S. A.; Mirkin, M. V. *Anal. Chem.* **2002**, *74*, 6340−6348.
(89) Kneten, K. R.; McCreery, R. L. *Anal. Chem.* **1992**, *64*, 2518−2524.
(90) McDermott, C. A.; Kneten, K. R.; McCreery, R. L. *J. Electrochem. Soc.* **1993**, *140*, 2593−2599.
(91) Rodríguez-López, J.; Minguzzi, A.; Bard, A. J. *J. Phys. Chem. C* **2010**, *114*, 18645−18655.
(92) Hurrell, H. C.; Abruña, H. D. *Anal. Chem.* **1988**, *60*, 254.
(93) OPA445 High Voltage FET-Input Operational Amplifier, Texas Instruments technical note. SBOS156B − March 1987 − Revised April 2008.
(94) These coverages are similar to others observed on cobalt complexes in related materials. McQueen, E.; Goldsmith, J. I. *J. Am. Chem. Soc.* **2009**, *131*, 17554−17556.
(95) Lefrou, C.; Cornut, R. *ChemPhysChem* **2010**, *11*, 547−556.
(96) Cobalt(II) bis-terpyridine is labile in highly acidic medium but shows negligible decomposition at neutral pH. Farina, R.; Hogg, R.; Wilkins, R. G. *Inorg. Chem.* **1968**, *7*, 170−172.
(97) Experiments (not shown) where reversible mediators (e.g., methyl viologen) that show quantitative positive feedback were used together with sluggish Fe(II/III) couples to calibrate their feedback response demonstrate that this positioning method is valid; a maximum error of $\sim \pm 1$ $\mu$m can be conceded.
(98) In this procedure, all experimental tip currents within a run were also divided by an arbitrary constant in order to fit them in the vertical axis. The overall procedure is equivalent (and was checked to be so) to comparing the normalized simulated result to a normalized experimental result at a fixed absolute time, except that in this case it is necessary to obtain a simulated curve for any possible value of $D$; this is less convenient than fitting the data by choice of $D$ to the master curve.
(99) Kneten Cline, K.; McDermott, M. T.; McCreery, R. L. *J. Phys. Chem.* **1994**, *98*, 5314−5319.
(100) Ishigami, M.; Chen, J. H.; Cullen, W. G.; Fuhrer, M. S.; Williams, E. D. *Nano Lett.* **2007**, *7*, 1643−1648.
(101) Reina, A.; Jia, X.; Ho, J.; Nezich, D.; Son, H.; Bulovic, V.; Dresselhaus, M. S.; Kong, J. *Nano Lett.* **2008**, *9*, 30−35.
(102) Gewirth, A. A.; Bard, A. J. *J. Phys. Chem.* **1988**, *92*, 5563−5566.
(103) Huang, P. Y.; Ruiz-Vargas, C. S.; van der Zande, A. M.; Whitney, W. S.; Levendorf, M. P.; Kevek, J. W.; Garg, S.; Alden, J. S.; Hustedt, C. J.; Zhu, Y.; Park, J.; McEuen, P. L.; Muller, D. A. *Nature* **2011**, *469*, 389−392.
(104) McDermott, M. T.; Kneten, K.; McCreery, R. L. *J. Phys. Chem.* **1992**, *96*, 3124−3130.
(105) Fodi, B.; Hentschke, R. *Langmuir* **1998**, *14*, 429−437.
(106) Levedeva, I. V.; Knizhnik, A. A.; Popov, A. M.; Ershova, O. V.; Lozovik, Y. E.; Potapkin, B. V. *Phys. Rev. B: Condens. Matter Mater. Phys.* **2010**, *82*, 155460/1−155460/10.